IEEE Sensors Council

Low-Cost Compact Integrated Rectenna for Implantable Medical Receivers

Saad G. Muttlak, M. Sadeghi, Kawa Ian and M. Missous, *Senior Member, IEEE*

Abstract— **This work describes a novel fully integrated rectenna circuit using tunnelling-based devices for implanted medical devices. An ASPAT (Asymmetric Spacer Layer Tunnel Diode) was used as the active rectifier due to its high non-linearity and temperature insensitivity features. A miniaturized geometry rectenna (1×5mm^2) with improved matching characteristics was demonstrated, by integrating a Cockcroft-Walton rectifier with an L-shaped planar folded antenna structure operating at ISM frequency bands. The circuit performance was experimentally explored at various separation distance between transmitter and receiver units. For a 5cm transmission set-up, the rectenna with a single-stage rectifier delivered 0.8V output at 20dBm transmit power. An extended doubler configuration exhibited enhanced performance when multiple stages are used, is predicted to reach 0.24mW output power at 23dBm transmit power and yielding ~1.6V output voltage with an efficiency of 0.12%. These findings can assist in compensating for the degraded antenna gain attributed to the extremely small effective-radiating area of 0.04λ. Furthermore, the ability of controlling the antenna input impedance helps in circumventing the requirement for a matching circuitry thereby offering further reduction in chip size.**

***Index Terms*—Planner folded antenna, wireless power transfer, biomedical implant devices, near-field RF powering, ASPAT-based circuits.**

I. Introduction

In recent years, a surge of interest in wireless sensor networks and implantable devices has occurred to meet the increased end-user demands in industrial and health care monitoring fields[1][2]. Smart implants are an effective monitoring technique for physiological signal sensing from human bodies and sending it to the patients and/or their medical doctors to be checked afterwards using a mobile application [3]. The possibility of communicating with implanted devices wirelessly has been reflected in a few available systems, such as brain-to-nerve interconnections for brain injury detections [4], monitoring of blood pressure in the brain cavity and retinal implants [5]. The issues to consider for in-body devices concern overall chip size, its power consumption and compatibility with medical treatment restrictions. Ultimate chip dimensions of <10mm^2-scale can be implanted by minor surgical treatment and the use of a zero-bias detector significantly minimizes power consumption of the system. The dimensions of the embedded electronic sensors in the system can be as small as <0.015mm^3[3], and thus the challenge emerges from miniaturization of the antenna. This in turn greatly limits the amount of received/transmitted RF power when operating in the authorized 433.1-434.8MHz, 902-928MHz, 2.4-2.5GHz and 5.8GHz band frequencies allocated for industrial, scientific and medical (ISM) fields [2]. Unlike low operating frequencies, the 2.4-2.5GHz radio band has a good compromise between acceptable penetration depth in human body tissue and antenna size with higher radiation power and longer communication range. According to Gabriel's parametric tissue models, a penetration depth of 8cm in infiltrated fat and 2cm in dry skin and muscle were found [6][7]. A conventional $\lambda/2$ dipole antenna operating at 2.4GHz has a length of 62.5mm but size reduction is feasible when high-k dielectric materials are used [8]. With modern on-chip antenna design, attainable dimensions are 1.5×2mm^2 and can be increased to at least 3×4mm^2 due to the special ground plane design requirements and associated bulky matching circuit [9].

A coplanar waveguide-fed antenna on ceramic substrate [10] and recently a planar inverted structure with reduced semi-circular shape were suggested for skin implantation in medical implant communications service (MICS) band [11]. However, these still suffer from large antenna dimensions of >9.5×19mm^2 and/or rectifier circuit integration difficulties. As such, dipole terminations, in which the ground plane is on the top of the substrate, for simplified subsequent rectifiers integration and testing procedure are preferred. A breakthrough 0.2×5.5mm^2 (diameter × length) implanted helical antenna, relying on self-assembly process was demonstrated [3]. This has not been yet experimented with a complete rectenna scheme and it further requires bonding process from the rolled-up antenna into the rectifier pads.

Therefore, planar folded antenna structure is a good candidate for implanted biomedical circuits benefiting from its miniaturized physical size, relaxed micro fabrication process

This research was supported by the European Union's Horizon 2020 research and innovation programme under grant agreement No 857654–UWIPOM2. "Ultra-Efficient Wireless Powered Micro-robotic joint (UWIPOM2)" and by the EPSRC through EP/P006973/1 "Future Compound Semiconductor Manufacturing Hub".

Saad G. Muttlak and M. Missous are with the Department of Electrical and Electronic Engineering, University of Manchester, Manchester M13 9PL, U.K. (e-mail: saad.muttlak@manchester.ac.uk)

M. Sadeghi is with Advanced Hall Sensors Ltd, Manchester, M17 1RW, U.K. Kawa Ian is with Integrated Compound Semiconductors Ltd, Manchester, M17 1RW, U.K.

and integration compatibility with semiconductor rectifiers. The full rectenna circuit can be then encased in a capsule and embedded into the human body with standard medical syringes, employing 16–19gauge needles with 1.6–1.1mm typical inner diameters [12]. This avoids medical surgery and any pain that may be caused after implantation.

Whilst a reduced antenna geometry is tailored to a specific application, it is critical to achieve adequate gain at ISM frequencies. It is necessary to improve the delivered power signal and/or operate within the near-field radiation distance for less transmission losses. Evidently, the near-field operation results in a decrease in the antenna gain. Many circuit topologies have been recommended for enhanced rectenna response, including voltage doublers in conjunction with broadband matching network and multistage doubler configuration [13][14]. A developed rectifier booster regulator with matching converters has been demonstrated using Greinacher and Cockcroft-Walton circuits [15]. The work reported here is dedicated to the design and experimental evaluation of a 2.4GHz reduced-sized rectenna for implanted devices. A single stage Cockcroft-Walton voltage doubler is designed using zero power dissipation ASPAT tunnel-based diodes. The temperature independent and zero-bias voltage characteristics of the diode are advantageous features for detectors in transceiver systems as demonstrated in previous work [16][17]. A miniaturized chip of dimensions 1×5mm^2 was achieved with optimized match-less network and a monolithically integrated rectenna circuit.

II. Antenna Design and Results

A folded antenna structure was constructed from two symmetrical radiating arms built with multiple L-shaped conducting sections. Fig. 1 shows a 1×5mm^2 folded antenna designed to resonate at the 2.4GHz ISM band. The use of open-ended arm formation is crucial in providing for antenna input impedance adjustment and size reduction features [18]. The variation in the main and folded arm widths (w_1 and w_2) can also dominate the real and imaginary part values of the antenna input impedance respectively. Furthermore, the resonant frequency can be determined from the l_1 to l_7 lengths and the arm-folding scheme offers miniaturized structure dimensions as studied in [19]. The antenna geometrical characteristic was investigated, starting from a single L-shaped arm and successively adding L-loading sections, this tunes out the capacitive behavior of the antenna input impedance as also demonstrated in [20]. The respective feeding gap length, d_1 and main arm stripline width, w_1 were chosen to be 0.04mm and 0.03mm as these are convenient for ground-signal on-wafer probing measurement techniques. The optimized conductor spacing, d_2 is 0.23mm which in turns yields sufficient area for the integrated rectifier circuit. Moreover, the folded stripline conductor width, w_2 and conductor spacing, d_3 are kept constant at 0.02mm in both arm sections. It is worth mentioning that the dependency of the antenna reactance, jZ_{Ant} on w_1 and w_2 can lead to delivering an inducive response at certain frequency bands. A value of 0.9mm is used for l_1 to allow 0.05mm spacing from each side of the antenna required for the final dicing-up process without damaging the antenna edges. The total trace length of a single arm section is 11.97mm including l_1 to l_7 and all other

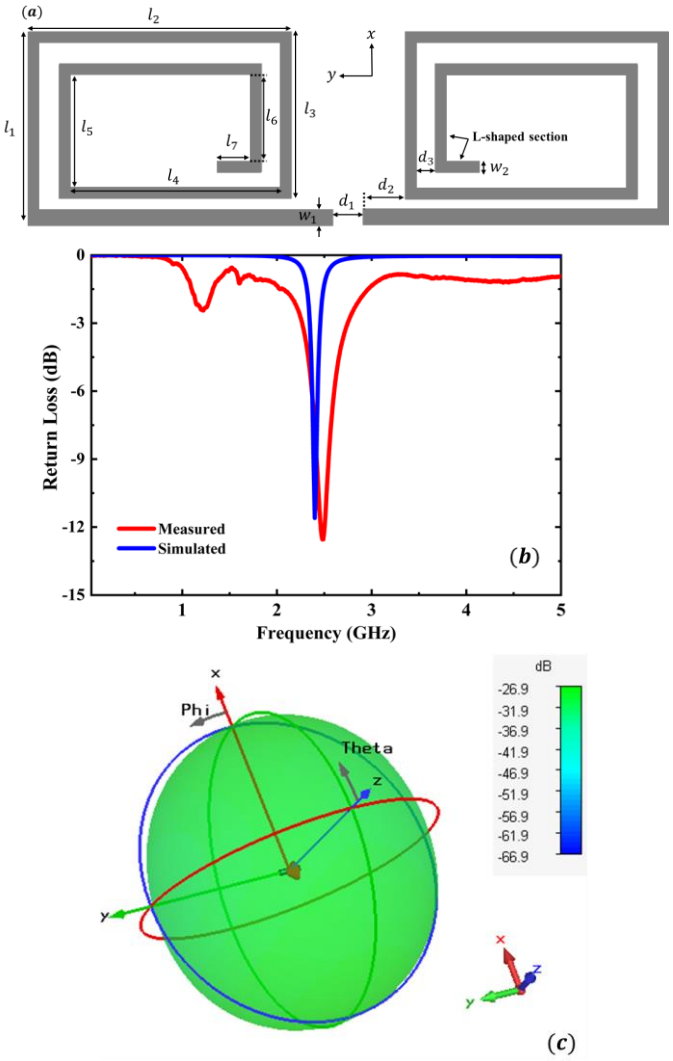

Fig. 1. (a) Geometry of a 1×5mm^2 four L-shaped folded antenna structure with relevant indicated dimensions (note that the drawing is not to scale), (b) Simulated and measured return loss results of the antenna and (c) Three-dimensional far-field antenna gain at 2.4GHz resonant frequency.

L-shaped lengths. In comparison with a 62.5mm $\lambda/2$ dipole antenna, the overall size reduction in the folded arm structure with four L-shaped sections is 92%. The antennas were designed on 0.625mm semi-insulating GaAs substrate with an ε_r =12.9 and loss tangent, tanδ =0.006 using CST-Microwave Studio. The antennas were fabricated afterwards using conventional i-line photolithography and wet etching processes.

Prior to measurement, a Vector Network Analyzer (VNA, Anritsu 37369A) was calibrated utilizing a short-open-load-thru (SOLT) calibration method to eliminate systematic errors for reliable and repeatable measurements. The experimental and simulated return loss response of a 50Ω feeding port antenna alongside its three-dimensional far-field gain is depicted in Fig. 1. The data exhibited good agreement and a measured 100MHz frequency bandwidth (BW) was evaluated at a reflection coefficient ($|S_{11}|$) below -10dB. Table I shows performance characteristics of the folded antenna with different dimensions and separation distances (d_2) as designed

to resonate at 2.4GHz. All other structure parameters were kept unchanged throughout the cases examined.

TABLE I
PERFORMANCE CHARACTERISTICS OF THE L-SHAPED FOLDED ANTENNA OPERATING AT 2.4GHZ FREQUENCY.

Size (mm^2)/No. of L-sections	d_2 (mm)	Z_{Ant} (Ω) (d_2=0.23)	$\|S_{11}\|$ (dB)	BW (MHz)	η_{rad} (%)
1×10/2.5	0.2/0.23	78+j138	-31/-26	55/52	0.57
1×8/2.5	0.2/0.23	128+j173	-16/-14.5	40/36	0.35
1×5/4	0.2/0.23	173+j264	-14/-12	33/28	0.13
1×3/10	0.2/0.23	203+j410	-14/-12	30/27	0.062

Of note, the antenna input impedance (Z_{Ant}) was extracted at ~2.45GHz operating frequency. It is observed that 1×10mm^2 antenna with 2.5 L-shaped sections has a 0.57% radiation efficiency, η_{rad}. The reduction in the antenna dimensions down to 5mm^2 has come at the expense of a -27dB gain with a severely degraded η_{rad} of 0.13%. An additional 48% drop occurs when a ten L-shaped 1×3mm^2 structure is used at similar operating frequencies. These are as expected due to the very small effective radiating antenna area designed here. Generally, the dipole geometry formation is accompanied by inevitable tradeoffs regarding small size, reasonable gain and radiation efficiency. However, the ISMs compact dimension constraints pave the way towards the realisation of extreme-downscaled planar antenna structures. In addition, the full rectenna output voltage level can be boosted to compensate for the deteriorated antenna performance.

III. RECTIFIER CIRCUIT ANALYSIS

A Cockcroft-Walton voltage doubler was used to overcome the low η_{rad} and gain of the antenna. The rectenna schematic comprising antenna, voltage doubler and load resistor is shown in Fig. 2. The doubler circuit is a composite of a voltage clamper (C_1 and D_1) and voltage peak detector formed by C_2 and D_2. In DC mode analysis, the ASPAT diode (D_1) is forward biased during the negative half-cycle (i.e., ideally short circuit) and the capacitor, C_1 is charged with an amplitude voltage of the received signal, V_m. For the positive half-cycle, the rectifying diode, D_2 is forward biased instead and C_2 will be holding $2V_m$, which simply doubles the resulting DC voltage. The C_1 capacitor also functions as an input bandpass filter to block the DC input component while V_{out} is smoothed by C_2 at the output terminals. In ac mode operation, C_2 is used to bypass the higher order modes to the ground, generated from the nonlinear characteristic of the zero-biased diode. The derived input impedance of the full doubler circuit can be expressed as:

$$Z_{in} = \frac{1}{j\omega C_1} + [Z_1] \parallel \left[Z_2 + \left(\frac{1}{j\omega C_2} \parallel R_L\right)\right] \quad (1)$$

Z_1, Z_2 are the input impedance of the two ASPAT diodes (D_1 and D_2) respectively. ω is the angular frequency in rad/sec, ω=2πf and f is the frequency. From the well-known equivalent circuit of ASPAT [19], $Z_{1,2}=R_s+(R_j/(1+j\omega C_j R_j))$, where R_s, R_j and C_j are the series resistance, junction resistance and junction capacitance of the equivalent circuit

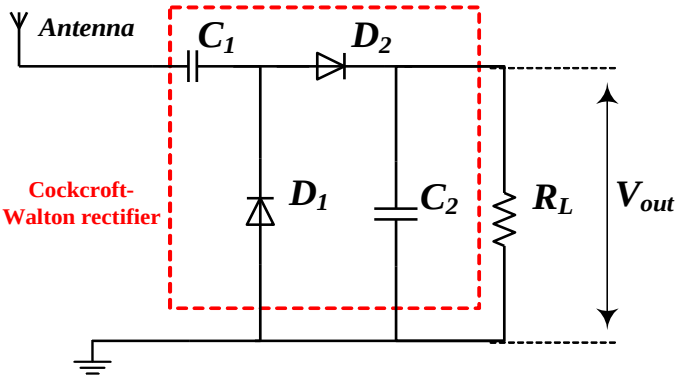

Fig. 2. Single stage Cockcroft-Walton voltage doubler circuit using integrated ASPAT diodes and folded antenna.

parameters. For sake of simplicity, $Z_{1,2}$ is multiplied by the complex conjugate of the second term to separate the real and imaginary components as formulated by $R_s+[R_j/(1+\omega^2C_j^2R_j^2)]-j[(\omega C_jR_j^2)/(1+\omega^2C_j^2R_j^2)]$. At the resonant frequency, the capacitor C_2 in (1) acts as a short circuit, thus the term $(1/j\omega C_2)\|R_L$ has a negligible effect on the impedance and (1) becomes:

$$Z_{in} = \frac{1}{j\omega C_1} + [Z_1 \parallel Z_2] \quad (2)$$

The doubler would have a corresponding impedance given by:

$$Z_{in} = \frac{R_s}{2} + \frac{R_j}{2 + 2\omega^2 C_j^2 R_j^2} - j\left(\frac{1}{\omega C_1} + \frac{\omega C_j R_j^2}{2 + 2\omega^2 C_j^2 R_j^2}\right) \quad (3)$$

ASPAT devices with a 10 monolayer (ML) AlAs thick barrier were grown on a GaAs substrate and then fabricated into different mesa sizes diodes. Six steps were conducted to successfully fabricate the devices and all active layers are protected by a thick passivation layer as the final processing step. A fitting approach for equivalent circuit parameter extraction with experimental S-parameter data up to 40GHz was performed as previously stated in [17]. The extracted junction resistance (R_j), junction capacitance (C_j) and series resistance (R_s) of a 6×6µm^2 ASPAT device at zero-voltage bias are 22.8kΩ, 71fF and 19Ω respectively. A maximum operating frequency of 118GHz is calculated using $f_{max}=1/\omega C_jR_j$, which can be extended further by downscaling the device geometry and/or optimizing the epilayer structure of the diode as discussed in [21].

From (3) and for 2.4GHz operating frequency, the rectifier has an approximated impedance of (29-j483)Ω at the given equivalent circuit parameters and 4pF C_1 charging capacitor. A comparable impedance value was found from harmonic balance simulation tool in ADS-software at an RF input power, P_{in} of -30dBm. Due to the small antenna area which restricts the amount of received power, Z_{in} is often

estimated at P_{in} exceeding 0dBm [22][23]. Fig. 3 (a). shows the variations of the real and imaginary components of

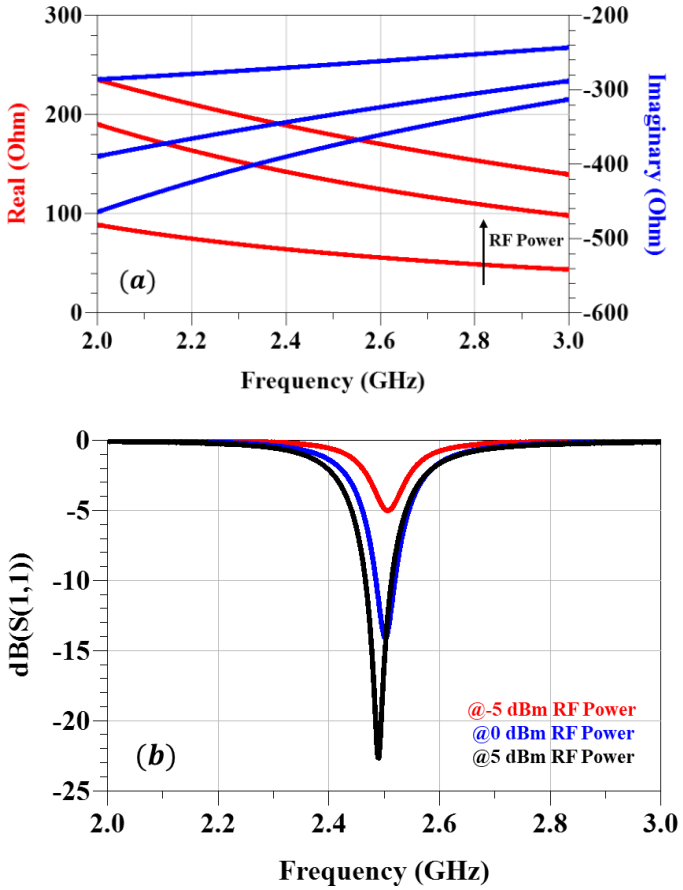

Fig. 3. (a) Real and imaginary parts of the rectifier input impedance (Z_{in}) as a function of frequecny at -5, 0 and 5dBm input power, (b) Reflection coefficient resposne of 1×5mm^2 four L-shaped folded antenna integrated with the voltage doubler circuit at -5, 0 and 5dBm input power.

the rectifier input impedance with different input RF power due to the nonlinear behavior of the diode I-V characteristic. To maximize available output voltage from the doubler, it is necessary to terminate the antenna with a matched impedance circuit. At this end, the rectifier becomes more resistive, *real(Zin)* and less capacitive, *imaginary(Z_{in})* with the drive input RF power and has an impedance of (180-j267)Ω at 5dBm. This is targeted to match the 1×5mm^2 four L-shaped antenna near the 2.48GHz ISM frequency band (i.e., $|jZ_{Ant} - jZ_{in}| \simeq 0$) as depicted in Fig. 3 (b). The antenna and rectifier circuit exhibited reasonable matching performance at a P_{in} of 0dBm as well. As such, this does not only decrease the reflection coefficient for better efficiency and overall performance but also enables match-less circuitry for compact doublers. In contrast, a conventional matching network design for the >200Ω capacitive reactance of the rectifier requires an inductive network occupying roughly 0.5mm^2. This is by the side of a poor Q-factor and self-resonant frequency of the inductors caused by the relatively large track length resistance and associated parasitic [24].

IV. Rectenna Architecture and Results

For propagation analysis, the key issue to consider is the dramatic decrease in RF signal level with distance, lowering the actual delivered power when an omnidirectional antenna is

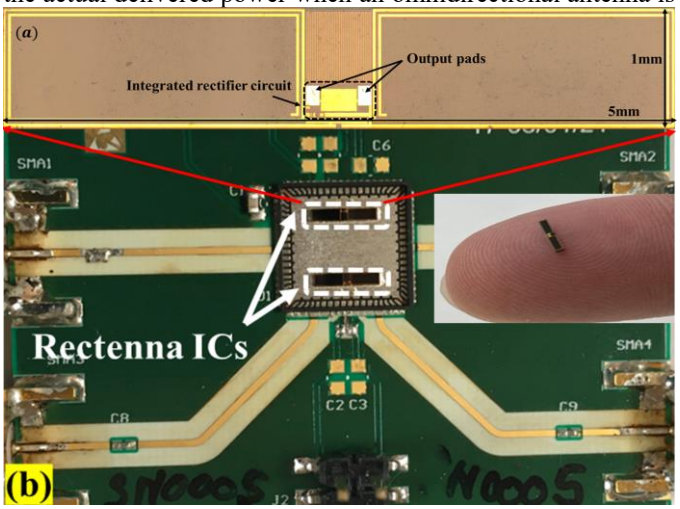

Fig. 4. (a) Microphotograph of the fabricated rectenna with a single-stage Cockcroft-Walton rectifier showing the compact full rectenna circuit, (b) The circuit is bonded into a QFN package from which the DC output voltage can be measured.

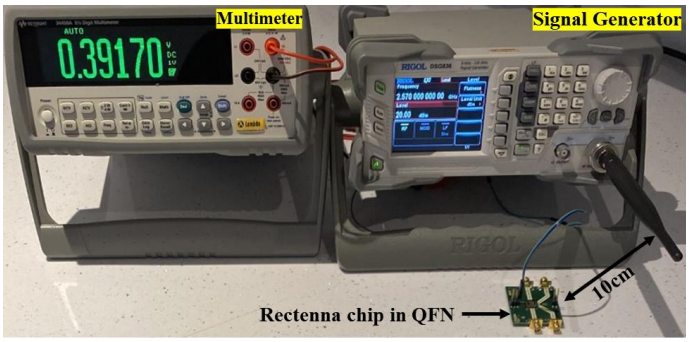

Fig. 5. Full rectenna integrated circuit measurement set-up showing the free-space test platform used in this work.

used. This limits the transmitter/receiver separation distance to a few tens of centimeters at which near-field radiation is mostly dominant. A careful consideration of path loss transmission and accompanying RF cables loss are vital for circuit performance evaluation. A DSG836 Rigol signal generator was employed and the received power was tested using a calibrated ML2438A Anritsu power meter. This showed that a 1dB loss is introduced through the cable. To measure the path loss, the RF power captured by an omnidirectional antenna can be assessed utilizing a transmitter and receiver antennas. For this aim, a 5dB gain swivel type antenna with 19.8cm physical length was used here, giving a rise to a near-field radiation distance of 65cm as found via [25]:

$$Near\ Field\ Distance \leq \frac{2D^2}{\lambda} \qquad (4)$$

Where D is the longest dimension of the antenna and the wavelength, λ is at the resonant frequency. A measured 20dB path loss at various transmit power, P_t (from 0 to 20dBm) was obtained when placing two swivel antennas 10cm away from each other. The high path loss observed here is due to the

naturally deteriorated transmitter/receiver characteristic by the near-field radiation impact. The monolithically integrated

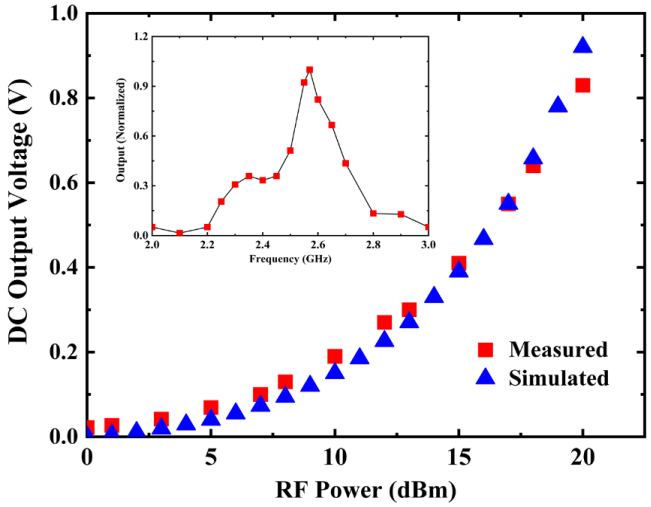

Fig. 6. Rectenna simulated and measured output voltage with a single stage rectifier circuit at 5cm transmission distance between the transmitter and receiver. Inset: Normalized output voltage as a function of source frequency at 20dBm transmitted power.

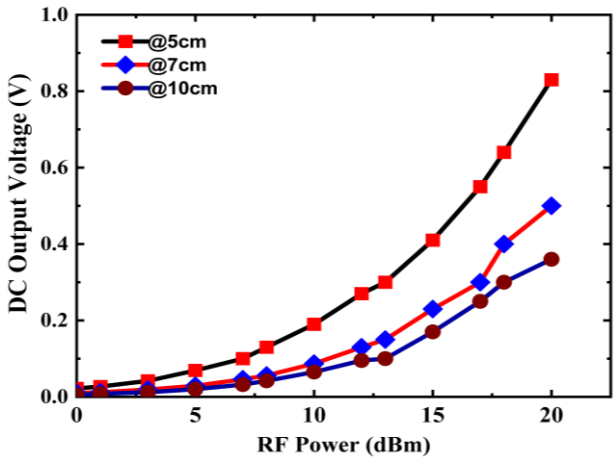

Fig. 7. Measured output voltage for rectenna circuit with a single stage rectifier circuit at different transmission distances.

rectenna circuit (depicted in Fig. 4) was placed into a QFN-package to facilitate the measurements set-up. The designed $0.1\times0.15mm^2$ signal-ground pads were bonded into the package hence allowing the measurements to be undertaken as shown in Fig. 5. The receiver was positioned at a 5cm distance and optimally angled to the transmitter to reduce multipath effects. The measurements started by sweeping the source frequency between 2 to 3GHz to determine the actual resonant frequency of the circuit, which was shifted to 2.57GHz. Fig. 6 shows the corresponding output voltage as a function of transmitted power.

The circuit delivered 0.8V DC output voltage at 20dBm (this power is the maximum that can be obtained from the signal generator used in this work) and agrees well with the simulation data when the total loss is taken into account. Several separation distances of 5, 7 and 10cm were explored as shown in Fig. 7. As expected, the voltage drops as the distance is increased due to the reduced power density of the propagated signal over the transmission distance. A 100kΩ spiral load resistor integrated in the circuit, R_L was chosen to maximize the DC output voltage. The system delivered 6.4μW

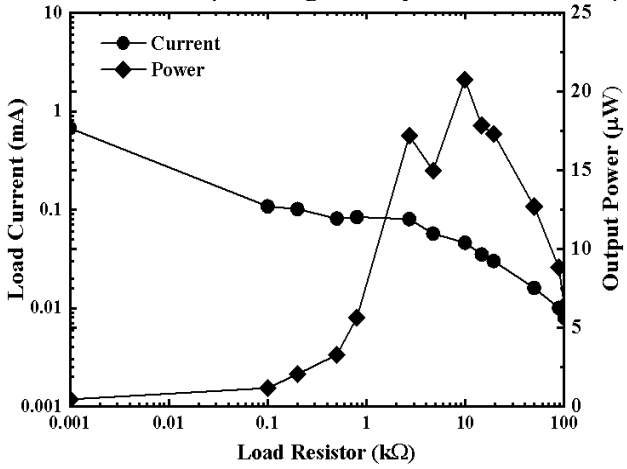

Fig. 8. Measured DC current and power for the recternna circuit with various load resistors at 5cm transmission distance.

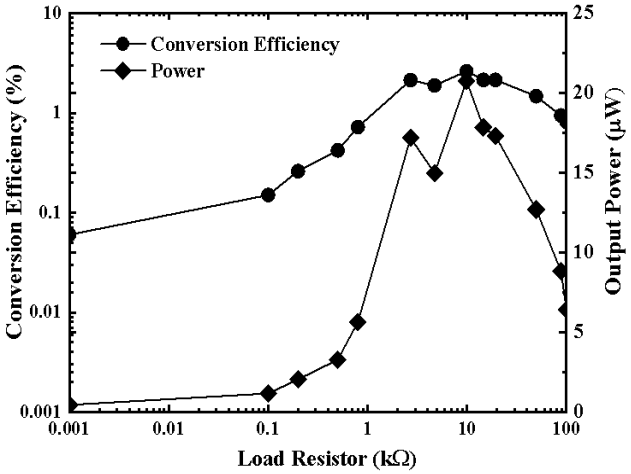

Fig. 9. RF-to-DC conversion efficiency and measured DC power for the recternna circuit with various load resistors at 5cm transmission distance.

DC power at the load and an obvious increase is predicted at P_t>20dBm. The circuit can still be tested up to P_t=35dBm in the near-field as the entire effective-isotopically radiated power, EIRP is 34dBm. The EIRP limit listed in FCC standards for a point-to-point link is 36dBm (~4W) at a maximum antenna gain of 6dB [27]. The substantial effect of the load resistor value on the circuit performance was studied to balance the trade-off between current and voltage at the output. Different load resistors were connected to the circuit which led to 0.1mA current at R_L=0.2kΩ. A maximum power of 21μW was found when using a 10kΩ load as shown in Fig. 8. A simulation with a higher transmit power of 23dBm yielded 0.13mW output power with an enhanced efficiency of 0.065% as calculated using (P_{DC}/P_t). Excluding the effect of path loss, the RF-to-DC conversion efficiency of the rectenna as a function of RL was obtained from the ratio P_{DC}/P_{in} as depicted in Fig. 9. The circuit has a conversion efficiency of 2.6% at an optimum load of 10kΩ and is expected to improve at higher P_{in}. To derive high load power and thus better conversion efficiency, a multistage Cockcroft-Walton rectifier is necessary. With the additional stage illustrated in Fig. 10,

TABLE II
FOLDED RECTENNA CIRCUIT FOR IMPLANTED DEVICES INVESTIGATED IN THIS WORK COMPARED WITH LITERATURE.

Reported in	Antenna/Rectifier Type	Circuit Area (mm^2)	Test Scenario	Separation Distance (cm)	Power Transmitted/Received	Full-Rectenna Efficiency (%)
[2]	Circular/Doubler	91.5	Implanted	40	1W/4.3µW	0.00043
[23]	Patch/Quadrupler	27.5×19.6	Free-Space (implantable envisioned)	42	44.5mW/1200µW	~2.7
[28]	Spiral/Single Diode	11×26	Implanted	6.5	0.5W/125µW	0.025
[29]	Square-Loop/(N/A)	6.8×6.8	Implanted	5-6	0.5W/120µW	0.024
This work	Folded/Doubler (1-stage)	1×5	Free-Space (Measured)	5	0.1W/6.4µW	0.0064
This work	Folded/Doubler (2-stages)	1×5	Free-Space (Simulated)	5	0.2W/240µW	0.12

the circuit integration capability into 1×5mm^2 chip size is feasible since the antenna structure design has a

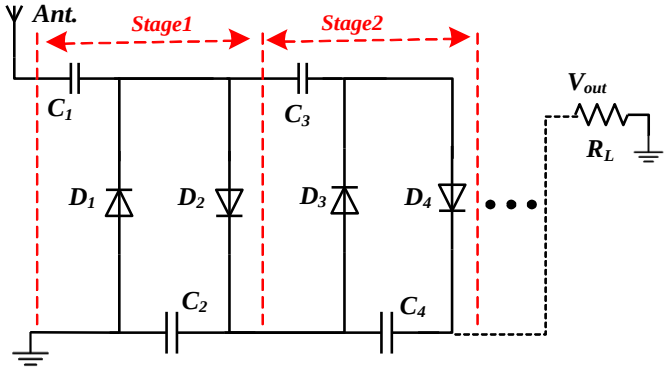

Fig. 10. Rectenna schematic circuit with multistage Cockcroft-Walton rectifier showing how the successive stage 2 are flipped over compared with stage-1 and are all connected to a unified ground.

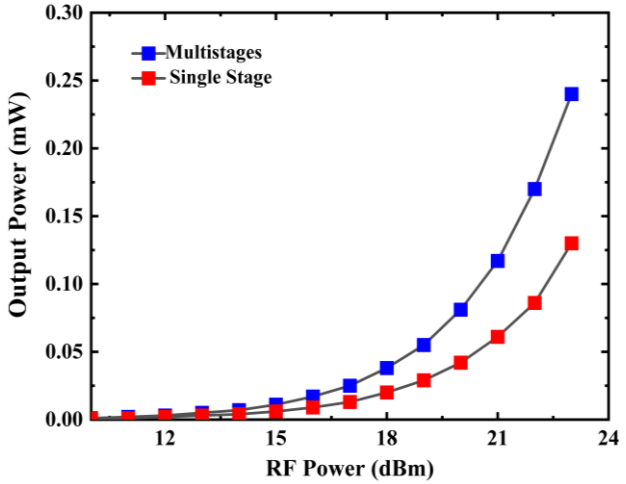

Fig. 11. Optimum load power for single and 2-stages rectifier circuits. The data ranges from 10 to 23dBm transmitted power.

0.23mm conductor spacing that allows sufficient area for a high yield processing. An increase in voltage is apparent when using three charging capacitors (C_1-C_3) without sacrificing the load current. The variation in the charging capacitors indicated that 4-5pF are adequate for proper circuit operation. The load was adjusted to 10kΩ for both stage configurations to acquire the highest possible power delivered. With two rectifier stages at 5cm Tx/Rx separation, the rectenna circuit is predicted to provide 0.24mW at 23dBm (V_{out} ~1.6V), which translates into a reasonable efficiency and RF-to-DC conversion efficiency of 0.12% and 15% respectively when compared with the literature as depicted in Fig. 11.

A comparison of the work described here with the state-of-the-art developed for biomedical implanted ICs is shown in Table II. The obtained DC power result from the single stage rectenna-doubler is higher than that stated in [2] despite the reduced folded rectenna area by >18 times. It is also suitable for several reported sensors in the literature, for instance a 0.07mm^2 size bladder pressure monitoring sensor was demonstrated with 0.3V supply voltage and 0.27µW power consumption [26].

V. CONCLUSION

This work presents a design, fabrication and associated results and analysis of a novel rectenna integrated circuit aimed at biomedical applications. A miniaturized folded antenna structure was demonstrated with simulated and experimental S_{11} data showing excellent agreements. A zero-voltage bias ASPAT diode has been successfully integrated, forming a doubler rectifier circuit. The optimized antenna geometry offered the ability to realize the full circuit without the need for a matching network. An in-house measured rectenna at 2.57GHz actual operating frequency delivered 6.4µW output power at 20dBm transmitted power. A simulated multistage rectifier circuit with optimum load and charging capacitors values is proposed to boost the output power. 0.13 and 0.24mW delivered power for single and multistage circuits can be achieved respectively. The reduced size, cost-effective manufacturing of the proposed rectenna as well as the excellent results obtained here should be appealing for implanted medical devices applications.

VI. ACKNOWLEDGMENT

This research was supported by the European Union's Horizon 2020 research and innovation programme under grant agreement No 857654–UWIPOM2. "Ultra-Efficient Wireless Powered Micro-robotic joint (UWIPOM2)" and by the EPSRC through EP/P006973/1 "Future Compound Semiconductor Manufacturing Hub".

REFERENCES

[1] M.-J. Nie, X.-X. Yang, G.-N. Tan, and B. Han, "A compact 2.45-GHz broadband rectenna using grounded coplanar waveguide," IEEE Antennas Wirel. Propag. Lett., vol. 14, pp. 986–989, 2015.

[2] S. Ding, S. Koulouridis, and L. Pichon, "Miniaturized implantable power transmission system for biomedical wireless applications," Wirel. Power Transf., vol. 7, no. 1, pp. 1–9, 2020.

[3] D. D. Karnaushenko, D. Karnaushenko, D. Makarov, and O. G. Schmidt, "Compact helical antenna for smart implant applications," NPG Asia Mater., vol. 7, no. 6, pp. e188–e188, 2015.

[4] Y. Li, M. Alam, S. Guo, K. H. Ting, and J. He, "Electronic bypass of spinal lesions: activation of lower motor neurons directly driven by cortical neural signals," J. Neuroeng. Rehabil., vol. 11, no. 1, pp. 1–12, 2014.

[5] D. Hodgins et al., "Healthy aims: Developing new medical implants and diagnostic equipment," IEEE Pervasive Comput., vol. 7, no. 1, pp. 14–21, 2008.

[6] T. Wu, T. S. Rappaport, and C. M. Collins, "The human body and millimeter-wave wireless communication systems: Interactions and implications," in 2015 IEEE International Conference on Communications (ICC), 2015, pp. 2423–2429.

[7] S. Gabriel, R. W. Lau, and C. Gabriel, "The dielectric properties of biological tissues: III. Parametric models for the dielectric spectrum of tissues," Phys. Med. Biol., vol. 41, no. 11, p. 2271, 1996.

[8] M. M.-U.-T. Chowdhury, M. M. Islam, and M. S. A. Bhuiyan, "Analysis and improvement of Si integrated on-chip dipole antennas using high-k dielectric materials for ultra-wideband signal transmission," in 2014 International Conference on Informatics, Electronics & Vision (ICIEV), 2014, pp. 1–6.

[9] D. J. Young, "Development of wireless batteryless implantable blood pressure-EKG-core body temperature sensing microsystem for genetically engineered mice real time monitoring," in 2009 IEEE 3rd International Conference on Nano/Molecular Medicine and Engineering, 2009, pp. 259–264.

[10] T.-F. Chien, C.-M. Cheng, H.-C. Yang, J.-W. Jiang, and C.-H. Luo, "Development of nonsuperstrate implantable low-profile CPW-fed ceramic antennas," IEEE Antennas Wirel. Propag. Lett., vol. 9, pp. 599–602, 2010.

[11] R. Li and S. Xiao, "Compact slotted semi-circular antenna for implantable medical devices," Electron. Lett., vol. 50, no. 23, pp. 1675–1677, 2014.

[12] P. R. Troyk, "Injectable electronic identification, monitoring, and stimulation systems," Annu. Rev. Biomed. Eng., vol. 1, no. 1, pp. 177–209, 1999.

[13] N. M. Roscoe and M. D. Judd, "Optimization of voltage doublers for energy harvesting applications," IEEE Sens. J., vol. 13, no. 12, pp. 4904–4911, 2013.

[14] W. Jung et al., "An ultra-low power fully integrated energy harvester based on self-oscillating switched-capacitor voltage doubler," IEEE J. Solid-State Circuits, vol. 49, no. 12, pp. 2800–2811, 2014.

[15] S. Fan et al., "A 2.45-GHz rectifier-booster regulator with impedance matching converters for wireless energy harvesting," IEEE Trans. Microw. Theory Tech., vol. 67, no. 9, pp. 3833–3843, 2019.

[16] M. R. R. Abdullah, Y. K. Wang, J. Sexton, M. Missous, and M. J. Kelly, "GaAs/AlAs tunnelling structure: Temperature dependence of ASPAT detectors," in 2015 8th UK, Europe, China Millimeter Waves and THz Technology Workshop (UCMMT), 2015, pp. 1–4.

[17] K. N. Z. Ariffin et al., "Investigations of asymmetric spacer tunnel layer diodes for high-frequency applications," IEEE Trans. Electron Devices, vol. 65, no. 1, pp. 64–71, 2017.

[18] S. Bakogianni and S. Koulouridis, "An implantable planar dipole antenna for wireless medradio-band biotelemetry devices," IEEE Antennas Wirel. Propag. Lett., vol. 15, pp. 234–237, 2015.

[19] S. G. Muttlak, M. Sadeghi, K. Ian, and M. Missous, "Miniaturized Folded Antenna with Improved Matching Characteristic for mm-wave Detections," in 2021 14th UK-Europe-China Workshop on Millimetre-Waves and Terahertz Technologies (UCMMT), 2021, pp. 1–3.

[20] S. Bakogianni and S. Koulouridis, "Design of a novel compact printed folded dipole antenna for biomedical applications," in The 8th European Conference on Antennas and Propagation (EuCAP 2014), 2014, pp. 3178–3182.

[21] A. Salhi, A. Hadfield, S. G. Muttlak, J. Sexton, M. J. Kelly, and M. Missous, "Design and analysis of GaAs/AlAs asymmetric spacer layer tunnel diodes for high-frequency detection," Phys. E Low-dimensional Syst. Nanostructures, vol. 130, p. 114723, 2021.

[22] H. Cheng, T. Yu, and C. Luo, "Direct current driving impedance matching method for rectenna using medical implant communication service band for wireless battery charging," IET Microwaves, Antennas Propag., vol. 7, no. 4, pp. 277–282, 2013.

[23] B. J. DeLong, A. Kiourti, and J. L. Volakis, "A radiating near-field patch rectenna for wireless power transfer to medical implants at 2.4 GHz," IEEE J. Electromagn. RF Microwaves Med. Biol., vol. 2, no. 1, pp. 64–69, 2018.

[24] Y. Cao et al., "Frequency-independent equivalent-circuit model for on-chip spiral inductors," IEEE J. Solid-State Circuits, vol. 38, no. 3, pp. 419–426, 2003.

[25] C. A. Balanis, Antenna theory: analysis and design. John wiley & sons, 2015.

[26] H. Danneels, K. Coddens, and G. Gielen, "A fully-digital, 0.3 V, 270 nW capacitive sensor interface without external references," in 2011 Proceedings of the ESSCIRC (ESSCIRC), 2011, pp. 287–290.

[27] "FCC Rules and Regulations | AIR802 | 2.4 & 5 GHz Bands." available: https://www.air802.com/fcc-rules-andregulations.html (accessed Jan. 21, 2022).

[28] R. Das and H. Yoo, "A multiband antenna associating wireless monitoring and nonleaky wireless power transfer system for biomedical implants," IEEE Trans. Microw. Theory Tech., vol. 65, no. 7, pp. 2485–2495, 2017.

[29] A. Abid et al., "Wireless power transfer to millimeter-sized gastrointestinal electronics validated in a swine model," Sci. Rep., vol. 7, no. 1, pp. 1–6, 2017.